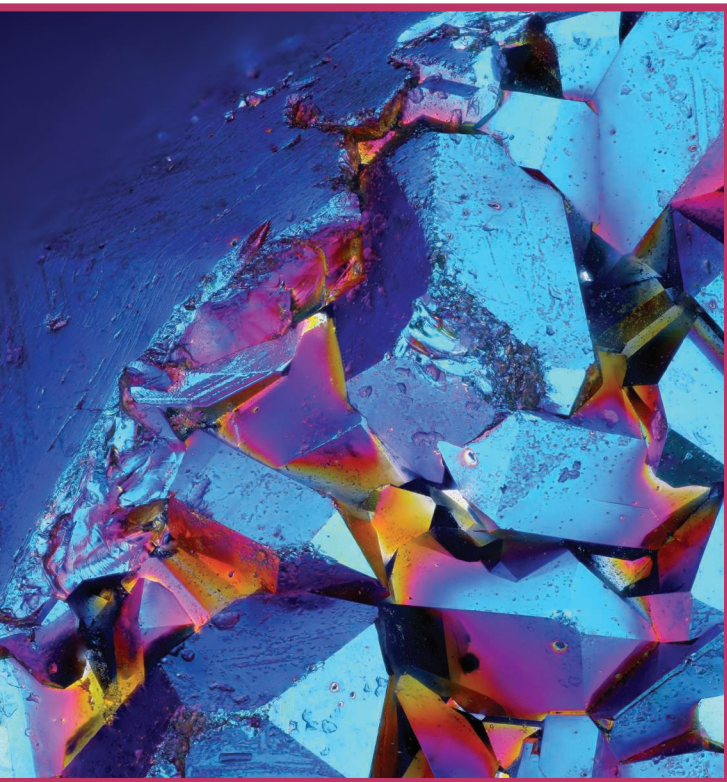


Lensless X-Ray Nanoimaging

Revolutions and opportunities



©SHUTTERSTOCK.COM/TOMATITO

Lensless X-ray nanoimaging provides 3D views of a wide range of materials with a spatial resolution better than 10 nm. These advances are enabled in part by dramatic gains in coherent X-ray flux, but they also rely on advances in signal processing to obtain images from coherent diffraction data. We outline the scientific problems that can be addressed by X-ray nanoimaging, the various imaging approaches and their associated reconstruction methods, and highlight opportunities for future advances.

Introduction

We are in an era of tremendous advances in methods for 3D nanoimaging. Electron tomography can be used to image nanoparticles at atomic resolution, but plural scattering effects begin to degrade the achievable spatial resolution as the sample thickness approaches $1\ \mu\text{m}$. In visible-light microscopy, sparse nanoparticles or switchable fluorophores can be localized to a few nanometers in sample layers approximately $1\text{-}\mu\text{m}$ thick, while confocal and multiphoton microscopy can be used for roughly 200-nm resolution on samples up to a few hundred-micrometers thick. However, X-rays are unique in offering penetration through millimeter-sized samples combined with a relative lack of plural scattering and nanometer-scale wavelengths to enable high spatial resolution [1]. The development of ever-improving synchrotron light-source facilities means that the available quasi-time continuous-coherent X-ray flux has been increasing for decades at a rate similar to Moore's law in electronics, as shown in Figure 1. High coherent flux has enabled a push in spatial resolution to below 10 nm [2] by providing sufficient photons for imaging fine, low-contrast features. Additional increases will allow for faster imaging, increased field of view, and the ability to go from imaging single-example specimens to gaining statistically significant insights from multiple specimens.

Much excellent work in X-ray nanoimaging is done using lenses such as Fresnel zone plates [3] or grazing incidence mirrors with multilayer coatings [4]. However, although X-ray optics reach 10-nm spatial resolution in some examples, they

still have a very low numerical aperture, limited field of view, and poor efficiency (often below 10%). One can largely bypass these optics-imposed limits through imaging based on the collection of far-field diffraction intensities, where one replaces the lens with a computer to form the image of the sample. In these coherent diffraction-imaging methods [5], the detector's pixel size can be tens of micrometers so that one can use direct detection in semiconductors for high efficiency and frame rate. Together, these advances in lensless X-ray nanoimaging are creating unprecedented opportunities for nondestructive studies in a wide range of fields, as described in the "Imaging Challenges in Materials Science" section and with a few examples shown in Figure 2.

These advances come with challenges and therefore new opportunities in signal processing for image reconstruction. X-rays are ionizing radiation, and basic models of imaging [6] imply that 10-nm-scale imaging involves imparting a radiation dose near 10^9 Gray (Joules/kg); although this is tolerated by most materials science specimens and even by biological specimens when cryogenic imaging conditions are employed, it still means that image reconstruction must deal with limited photon statistics. The combination of fine transverse resolution and high thickness demands 3D imaging, often with practical limits on the number of illumination directions when performing tomography. High coherent flux provides the opportunity to study dynamic changes in radiation-tolerant specimens, such as the flow of lithium-ion battery charge cycles [2]. Most techniques require scanning and rotating the specimen in the coherent beam, both of which are challenging at the nanometer-length scale; therefore, image-reconstruction methods must account for errors between the assumed and actual scanned positions and angles. Both phase and absorption contrast must be accounted for, with phase contrast increasingly dominant as the photon energy increases above 1 keV. Energy tunability can be used to carry out imaging around X-ray absorption near-edge resonances, providing the ability to see changes in the chemical binding state of many elements. Most importantly, when collecting diffraction intensities, one has the magnitude but not the phase of the far-field wavefield, so phase-retrieval methods must be used to recover the wavefield, and from that the object's optical transmissivity and thus its structure.

Here we outline the opportunities for insights into materials that lensless X-ray nanoimaging can provide. Realizing these opportunities will require advances in signal processing for reconstructing 2D and 3D images using far-field coherent diffraction data. Our goal is to summarize some of the important milestones rather than provide a comprehensive list of advances in the field. Although the original approaches were based on physics intuition, numerical optimization methods have been introduced, which now provide sufficient flexibility to handle the aforementioned complicating factors as well as incorporate a priori knowledge and assumptions regard-

ing the experiment and material under study. In fact, signal processing loops back to allow one to rethink the design of the experiment, creating revolutions and opportunities in nanoscale imaging.

Imaging challenges in materials science

The ability of X-rays to penetrate thick samples while also enabling high spatial resolution enables the study of hierarchical materials. A classic example is bone, which combines nanoscale arrangements of collagen and mineralized tissue with macroscopic changes in organization [10]. Integrated circuits offer another example [8], as depicted in Figure 2(b), as they have nanoscale arrangements of oxide layers at transistor gates but an overall organization that can extend to millimeters. Multiscale imaging is also required to study improved, low-carbon-emission types of cement [11]; improved alloys for strong, lightweight structural materials [12]; new materials for microelectronics

When studying beam-sensitive materials like biological cells and tissues, radiation damage is a significant consideration.

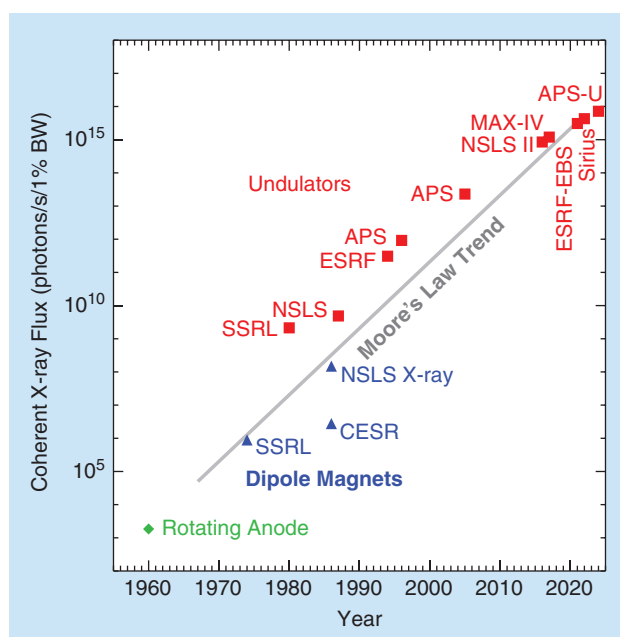


FIGURE 1. The coherent X-ray flux available from various multikeV sources over time. The green marker represents a standard X-ray rotating anode, the blue triangles represent dipole magnets at early synchrotron light sources, and the red squares are for undulators at synchrotron light sources (only a few representative facilities are shown; one can see a listing of all facilities worldwide at www.lightsources.org). The actual flux utilized is often considerably lower due to finer spectral filtering, beam-delivery optics inefficiencies, and other factors. Also shown is the trend of doubling every 18 months, which is the scaling of Moore's law for integrated circuit transistor count. Not shown here is the coherent flux available from X-ray free-electron lasers, which offer even higher flux; however, due to high intensity and low duty cycle, they are often used for single-shot imaging methods where the sample ends up destroyed. SSRL: Stanford Synchrotron Radiation Lightsource; CESR: Cornell Electron-Positron Storage Ring; NSLS: National Synchrotron Lightsource; ESRF-EBS: European Synchrotron Radiation Facility-Extremely Brilliant Source; MAX-IV: Microtron accelerator for X-rays-IV; BW: bandwidth.

[13]; and functional materials, such as for energy storage and conversion [14].

X-rays can also be used to provide important spectroscopic information within images. Outer-lying electron orbitals can be affected by the binding state of an element as well as by spin interactions in magnetism, so by tuning onto a resonance for exciting inner-shell electrons to these orbitals, one can look at changes in iron atoms as lithium atoms move during battery cycling [2], changes in carbon binding in organic photovoltaics [15], and internal domains in magnetic materials with ptychographic tensor tomography (where one obtains per-voxel measurements not just of a single variable like electron density, but of multiple variables, such as magnetic domain strength and orientation) [16].

When studying beam-sensitive materials like biological cells and tissues, radiation damage is a significant consideration. Especially for hydrated organic materials, cryogenic sample preparation and imaging conditions offer both the preservation of elemental content and structural detail in a close-to-living state, and sufficient radiation damage resistance to obtain high-resolution images, as shown in Figure 2(a). When the coherent beam is focused to a sufficiently small spot, one can collect not just the far-field diffraction pattern as required for ptychography but also X-ray fluorescent photons, allowing for simultaneous imaging of intrinsic elemental distributions [7].

The aforementioned examples involve absorption and phase modulation of the transmitted X-ray beam by the material under study. However, ptychography can also be carried out on the beam that is Bragg diffracted from a crystalline domain [17], with an example presented in Figure 2(c). Applications include the study of strain distribution in semiconductors, which affects electron mobility.

Image-reconstruction models and algorithms

Regardless of the application area or material type, the imaging process requires solving a set of inverse problems, such as phase retrieval or those that arise in tomography for reconstructing the sample from raw measurements. Over the past

few decades, both ptychographic phase-retrieval and tomographic image-reconstruction methods have advanced in parallel. However, today, we are seeing a merger of these two techniques for materials imaging, especially for 3D applications. The image-reconstruction problem in this setting boils down to reconstructing the sample from a set of detector intensities collected at different scan positions and beam

directions. This involves the phase-retrieval problem, which aims to recover the missing phases of the recorded data from diffraction-plane magnitudes, and the tomography problem, which seeks to regain the sample from its projections (usually represented by retrieved phases). Although there are numerous methods used to solve these problems, here we mostly highlight the approaches that have demonstrated massive success in practical applications and in turn revolutionized materials science.

Classical methods in coherent diffraction imaging

Motivated by protein X-ray crystallography to determine the atomic structure of biomolecules, early techniques focused on recovering the phase of the wave from a single diffraction pattern measurement. When a small sample can be isolated on a transparent membrane and the forward-scattered coherent diffraction pattern is collected [18], or when a small crystalline domain produces coherent diffraction about a Bragg peak [19], one has the most basic form of coherent diffraction imaging (CDI). The corresponding problem of recovering a signal from the magnitude of its

A generalized form of the HIO algorithm, also known as the *difference map*, allows one to control convergence through a relaxation parameter.

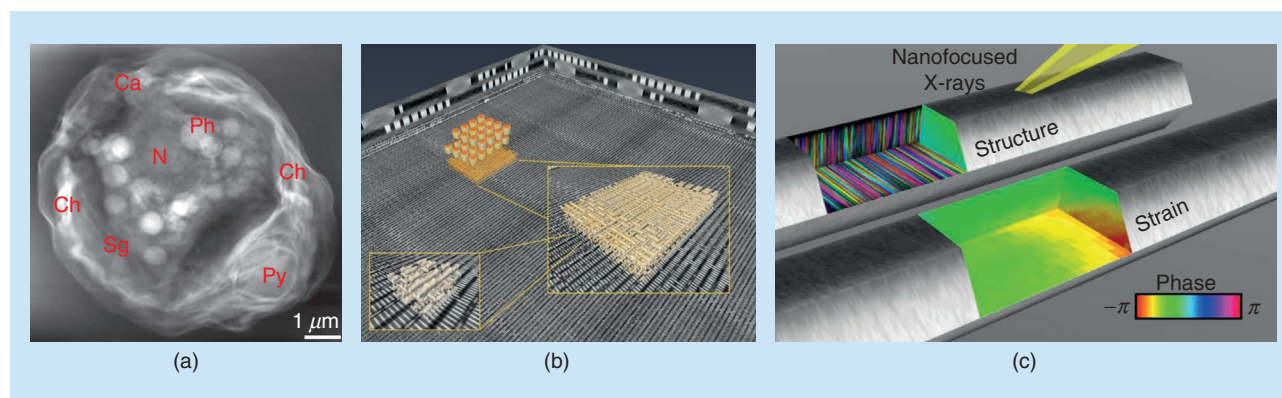


FIGURE 2. Lensless X-ray nanoimaging has an impact on a wide range of scientific disciplines. (a) A frozen hydrated alga cell imaged in 2D at an 18-nm resolution [7], including a single cup-shaped chloroplast (Ch) and a number of other organelles: pyrenoid (Py), nucleus (N), starch granule (Sg), and polyphosphate bodies (Ph). (b) The metallization layers from an integrated circuit imaged in 3D at a 19-nm resolution, with the ability to carry out a multiscale analysis [8] (Source: M. Holler, Paul Scherrer Institut, Switzerland; used with permission.) (c) An indium gallium arsenide nanowire imaged using multiangle Bragg projection ptychography with a 50-nm spatial resolution in 3D and a 2.6-nm resolution along the wire axis, where the stacking defects and strain can be mapped in 3D [9].

Fourier transform requires solving nonlinear equations of the form $d = |\mathcal{F}\psi|$, where d is the far-field diffraction magnitude measurements, \mathcal{F} is the Fourier transform, and ψ is the unknown signal (complex wave) that represents the sample's 2D transmission function (see Figure 3 for an illustration of the measurement process).

A particularly successful approach to solving for ψ is based on the Gerchberg–Saxton algorithm [20], leading to derived methods known as the *error reduction (ER)* and *hybrid input–output (HIO) algorithms* [21]. These schemes attempt to solve the following feasibility problem:

$$\text{find some } \psi \in O \cap D, \quad (1)$$

where O and D are sets that satisfy specific signal constraints in object (sample) and data spaces, respectively. Because the phase information is missing in measurement data, additional constraints are necessary to pick the desired solution among infinitely many solutions that agree with the measurement data. The approach requires alternating between feasible points in sets O and D until we reach a fixed point. In each iteration, we choose the locally optimal solution in each set among all locally optimal solutions. For example, the ER algorithm tries to solve the problem recursively by computing

$$\psi^{n+1} \leftarrow P_O P_D \psi^n, \quad (2)$$

where P_O and P_D are projection operators onto sets O and D , respectively, or

$$D = \{\psi : |\mathcal{F}\psi| = d\} \quad (3)$$

$$O = \{\psi : \psi \cdot 1_S = 0\}, \quad (4)$$

where $1_S : B \rightarrow \{0, 1\}$ is an indicator (also known as the *compact support*) function of subset S of B . Additional sets, such as positivity, can be used to appropriately constrain the solution space, depending on the problem. The advantage of this approach is that new sets of constraints can be easily added to the problem so that it is practical. Also, its implementation in software is straightforward because of the modular flow imposed by independent projection operations. However, when one of the constraint sets is nonconvex, such as the magnitude constraint set in (3), the algorithm can stagnate to a local solution or may not converge at all.

A more robust variant of the ER algorithm, the HIO one, provides a better convergence rate and can ameliorate some of the stagnation problems [see Figure 4(b) for a graphical illustration]. The iterate sequence of HIO differs from ER in that it involves reflection operators of the form $R_O = (2P_O - I)$ or $R_D = (2P_D - I)$ to avoid getting stuck in a local solution. Although the sequence generated by HIO does not necessarily involve a feasible point in any of those sets, often it gradually

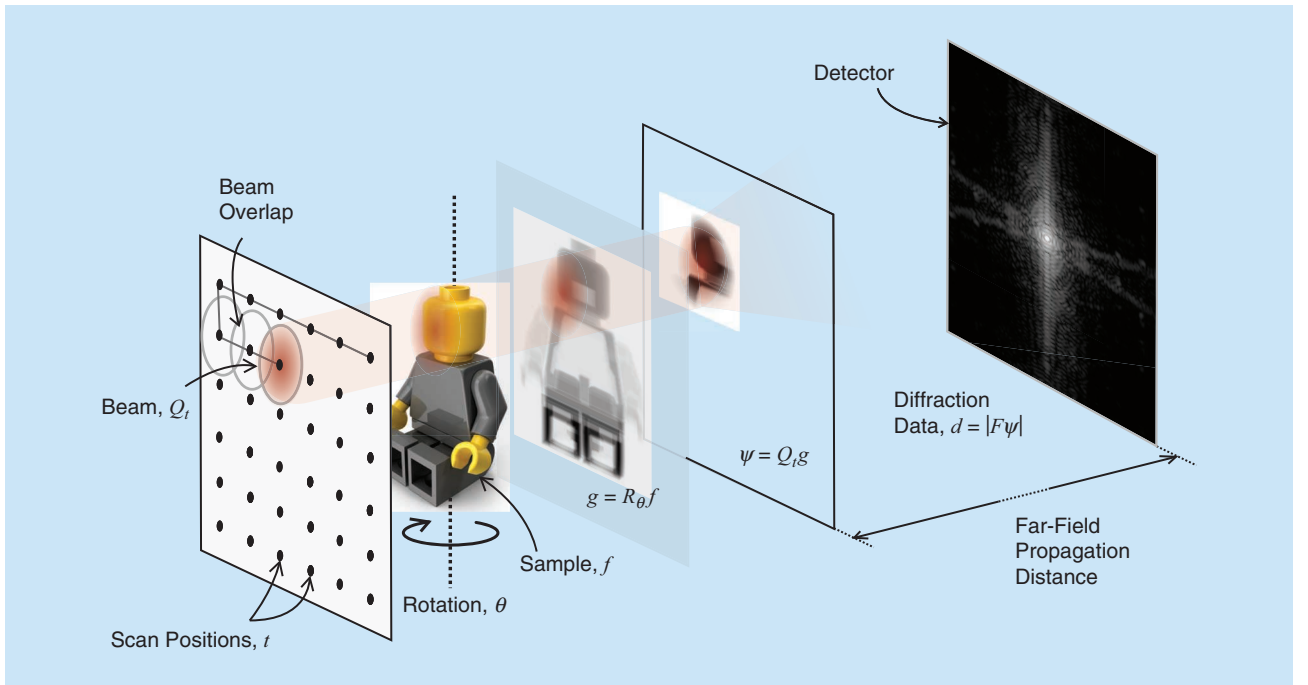


FIGURE 3. An illustration of the measurement process. A coherent beam of X-rays is modulated using the sample's transmission function g as a result of the traversing through sample f . The modulated signal ψ is then propagated in free space to the detector plane at the far field to measure signal amplitudes, which can be expressed through $d = |\mathcal{F}\psi|$. When the sample is smaller than the beamwidth, one has the most basic form of CDI and no scanning is required; however, for imaging large or thick samples, one can collect data at multiple beam positions t and sample rotations θ . The scanning process can be expressed by $\psi = Q_t g$, where Q_t is the beam at position t , and $g = R_\theta f$ is the object's 2D projection (or transmission function) along the beam path at rotation angle θ .

reduces the distance to the solution and has a more robust convergence behavior. The iterates of the HIO algorithm can be written as

$$\psi^{n+1} = \frac{1}{2}(I + R_O R_D)\psi^n, \quad (5)$$

where n is the iteration number. A generalized form of the HIO algorithm, also known as the *difference map (DM)* [22], allows one to control convergence through a relaxation parameter. Both HIO and the DM have been popularized in phase retrieval due to their scalability, superior performance, and easy implementation. It is noteworthy that those types of methods share similarities with projection onto convex sets (POCS) [23] or Douglas–Rachford algorithms [24]. They also have counterparts in convex optimization theory, especially with coordinate descent and other types of first-order schemes.

2D imaging of extended samples through scanning

The imaging of extended samples beyond the size of the illuminating beam is possible through ptychography, which replaces the finite support constraint of the object in single-particle CDI with finite support on a scanned coherent beam spot. Inspired by the success of ER and HIO algorithms, early studies focused on adapting those algorithms to ptychography by replacing the compact support constraint in CDI with the beam overlap constraint in ptychography. In ptychography, we can redefine sets D and O , respectively, as

$$D = \{\psi : |\mathcal{F}\psi| = d\} \quad (6)$$

$$O = \{g : Q_t g = \psi\} \quad (7)$$

and try to find g and a set of waves ψ that satisfy the constraints in both sets for all scan positions. Here Q_t is the beam used to sample ψ at positions t , and g is the object's

2D projection along the beam path. In this scenario, D is the Fourier-magnitude constraint set like in CDI, and O is the set that satisfies the overlap constraint from all scan positions. We can apply either the ER or HIO algorithm by defining P_D as the Fourier-magnitude constraint (similar to the CDI problem), and P_O as the minimizer for the least-squares problem, leading to $\min_g \|Q_t g - \psi\|_2^2$ for projection onto O in (7). In the context of ptychography, the ER implementation is often referred to as the *ptychographic-iterative engine (PIE)* [25], and the HIO implementation is called the *DM* (with a specific relaxation parameter) [26]. Both algorithms share a similar updating strategy, with the exception that in the PIE, set O is split into many subsets for each scan position, and the projection onto these subsets is done in a sequential fashion instead of simultaneously, as in the case of the DM.

Blind ptychography

Although one can measure the illumination (i.e., the probe) in ptychography beforehand, in practice, both the probe and the sample transmission function [Q and g , respectively, in (7)] can be recovered as a part of the reconstruction process. In this case, because ψ is dependent both on Q and g , there are many combinations that satisfy the constraint $Q_t g = \psi$. The common practice is to start the iterations with a probe function close to its solution (for example, from a previously measured probe); otherwise, the sequence often yields an undesired solution. Especially in CDI, because the measurements in the Fourier domain are insensitive to shifts of the signals in the sample domain, a global drift in sample and probe locations can happen. To circumvent this, additional constraints can be enforced to maintain stability and convergence. For example, the mass of the probe function can be enforced to stay in the center of the recovered images. This problem of solving both the sample and the probe, also known as *blind ptychography*, can be addressed by adding a probe-retrieval step when satisfying the constraint set in (7). A similar alternating solution strategy,

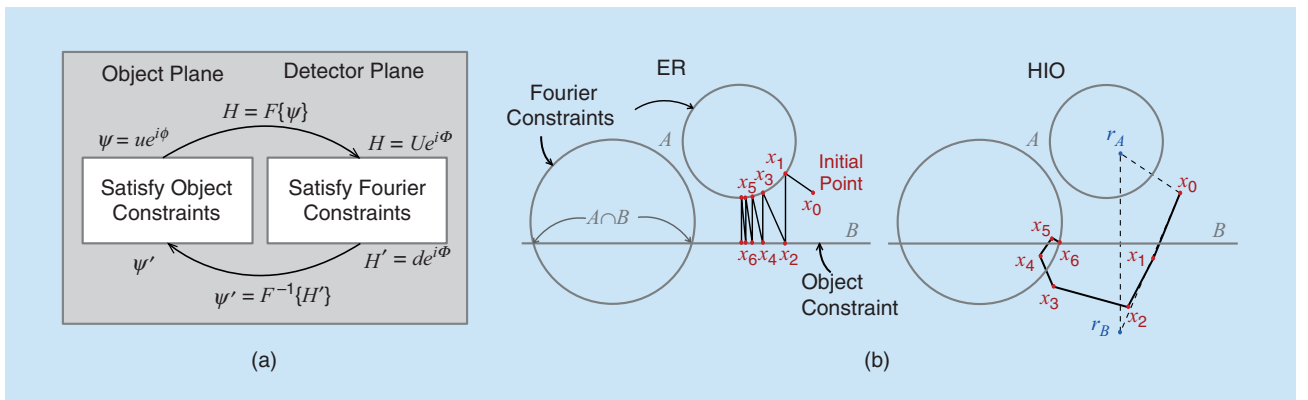


FIGURE 4. (a) A block diagram of the Gerchberg–Saxton algorithm [20]. A complex wave is transformed back and forth between the two domains, alternately satisfying the constraints (e.g., simulated wave H is altered by replacing its amplitude with measured amplitude d while keeping its phase to satisfy the Fourier constraint). (b) The convergence behavior of the ER and HIO algorithms [21] is graphically illustrated. In both algorithms, a sequence (x_0, x_1, x_2, \dots) is generated, applying projections onto set A (Fourier constraints) and set B (other constraints) alternately until we reach a fixed point. The ER can be trapped in a local solution or may not converge, as shown. The HIO can escape from local solutions and overcome the stagnation issues of ER. Note that the update rule of HIO involves computing two consecutive reflections (r_A and r_B) across sets A and B .

where one sequentially updates the sample image followed by the probe function, can be used in the DM [26] or the PIE [27] [the latter is called *extended PIE (ePIE)*]. There are additional strategies based on using optimization theory [28].

Imaging of thick samples in 3D

With the advent of undulators to create high coherent flux at high X-ray energies, one can perform a series of ptychography experiments on a 3D sample, followed after each series by a rotation so as to collect data in a tomographic setting. This marriage of ptychography and tomography enabled imaging the 3D structure of thick samples without sectioning. Beginning with the first demonstration approximately a decade ago [10], ptychotomography has continued to broaden its application areas in numerous materials research fields. The current mainstream approach includes solving a series of ptychographic phase-retrieval problems to find projection images at distinct angles, followed by a tomographic reconstruction to find the 3D structure of the sample. However, knowing that all the measurements are correlated and based on the 3D sample under study, jointly solving all problems at once can provide better stability or lead to compressive sampling strategies to save the radiation dose or data-acquisition time [29].

Separate solutions

Because ptychography and tomography problems are cascaded, one can separately solve them in a sequential manner, as noted previously. However, one can change the order of cascaded solutions, or use a joint approach. The reconstruction of 3D optical modulation f (the sample) for a given g can be obtained by finding a feasible point in the following set:

$$X = \{f : R_{\theta}f = g\}, \quad (8)$$

where R_{θ} is the X-ray transform that maps the 3D sample to its 2D projections at a given set of rotation angles θ . As an analytical inversion method with adequately sampled data, the filtered-backprojection scheme is often the technique of choice, but computationally more demanding iterative-optimization approaches are also becoming popular by solving problems of the form $\min_f \|R_{\theta}f - g\|_2^2$ (often with additional regularization terms to avoid reconstruction artifacts due to undersampling and measurement noise). It is again worth noting that iterative approaches such as the widely known algebraic reconstruction technique (ART) and simultaneous iterative reconstruction technique (SIRT) in tomography are particular instances of the POCS algorithm and are related to the ER and HIO algorithms in ptychography. An ART is similar to the ER or PIE algorithm in the sense that it uses successive projections onto many sets, where each set is a hyperplane defined by the measurement at an angle. Unlike an ART, an SIRT performs projections in all sets simultaneously, and the average of these projections is

used to update the point; it therefore shares similarities with the HIO or the DM algorithm.

Although regularization techniques can be employed to further constrain the solution set, the fundamental shortcoming of any separated-solution approach to the ptychotomography problem is that the resulting reconstruction errors in the phase-retrieval problem are propagated into the tomographic reconstruction problem. To avoid this propagation of errors,

experiments are sometimes designed such that the ptychography data for each angle are relatively oversampled and the tomography data are relatively undersampled. In other words, with the separated-solution approach, the imaging performance is bounded by the operation of the ptychography problem, which is solved prior to the tomography problem. To overcome the shortcomings of this solution strategy, especially for the case of incomplete and noisy

data, new approaches propose posing the problem as a joint optimization problem for extra robustness [29].

Joint solutions

The main advantage of a joint-solution approach [like the one demonstrated in Figure 5(a) and (b)] is that it requires less stringent data collection conditions by leveraging correlations among all measurements. As a result, data-sampling requirements for individual ptychography and tomography problems can be chosen to be more balanced. This helps with effective use of the dose fractionation theory [31], which states that one can take the exposure required to see the feature of a specified size and contrast in a 2D image and divide that exposure up among the set of tomographic projections. This is especially important for the X-ray ptychographic tomography of biological

Beginning with the first demonstration approximately a decade ago, ptychotomography has continued to broaden its application areas in numerous materials research fields.

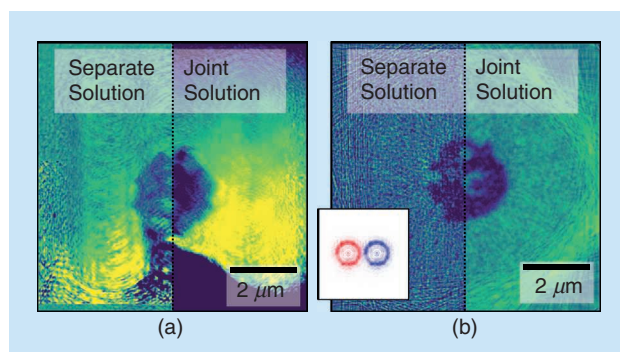


FIGURE 5. The reconstructions of (a) g and (b) f of a macroporous zeolite particle and probe with marginal probe overlaps (see the zoomed-in image for probe reconstructions at consecutive locations) [30]. The joint solution is more robust to data undersampling compared to a separate-solution approach, and it yields better quality reconstructions as the number of data points is reduced. Because the joint solution makes use of the angular-probe overlap inherent to tomographic acquisition, the lateral-probe overlap requirement in ptychography can be relaxed or almost completely lifted. (Source: M. Kahnt, Lund Universitij, Sweden; used with permission.)

specimens, where cryogenic preparation and imaging conditions are often used.

One of the first implementations of a joint formulation [29] used an ER algorithm approach by iteratively projecting onto the following sets:

$$D = \{\psi : |\mathcal{F}\psi| = d\} \quad (9)$$

$$O = \{g : Q_t g = \psi\} \quad (10)$$

$$X = \{f : R_{\theta} f = g\} \quad (11)$$

with an iterative scheme of

$$f^{n+1} \leftarrow P_X P_O P_D f^n. \quad (12)$$

Here P_D is the standard magnitude projector that replaces the amplitude of $\mathcal{F}\psi$ with d while keeping its phase, and P_O and P_X are often defined as the minimizers of the corresponding least-squares problems of $\min_g \|Q_t g - \psi\|_2^2$ and $\min_f \|R_{\theta} f - g\|_2^2$ respectively. Because generating this sequence requires solving two minimization problems for each iteration which is computationally demanding, approximate solutions (e.g., a few gradient descent iterations) are often sought, in practice, to improve performance. Splitting the projection operators also has some numerical benefits, by isolating the nonconvex set in (9) from convex sets in (10) and (11). For example, one can use different projection operators or algorithms to better control the convergence rate or reconstruction accuracy. Instead of using a DM (or Douglas–Rachford) sequence, one can also use other types of variable-splitting techniques, such as alternating method of multipliers [32] or proximal algorithms [33], which can improve or provide more stability to convergence.

Experimental uncertainties and limitations

As the transverse spatial resolution is pushed further into the nanoscale, experimental challenges such as limited photon flux, limited depth of field, and limited coherence of the illumination source, lead to problems with reconstructing the images. Furthermore, mechanical vibrations due to scanning become more apparent, limiting the achievable resolution in reconstructions. Therefore, we devote the following sections to highlighting the main solution approaches under realistic data-acquisition conditions.

Measurement noise

Although most studies use least squares as the projection operator onto sets (such as $\min_g \|Q_t g - \psi\|_2^2$ and $\min_f \|R_{\theta} f - g\|_2^2$), a parameterized random model such as the Poisson process can be preferred to accurately model the photon-counting process in the detector. Porod's law in small-angle scattering explains how X-ray diffraction strength decreases roughly with the fourth power of the scattering angle, which means that the detector pixels far from the optical axis record very small numbers of photons [1]. Therefore, a Poisson model is often the method of choice to improve accuracy of the model. This leads to a minimization problem in the form

$$\min_u \left\{ \sum_{k=1}^M (u_k - d_k \log u_k) \right\}, \quad (13)$$

where u is the expected set of diffraction intensities. Machine learning (ML) estimators are used both for ptychography [35] and ptychotomography [36], leading to superior results, as shown in Figure 6. Note that similar operator-splitting approaches can be applied to break the minimization

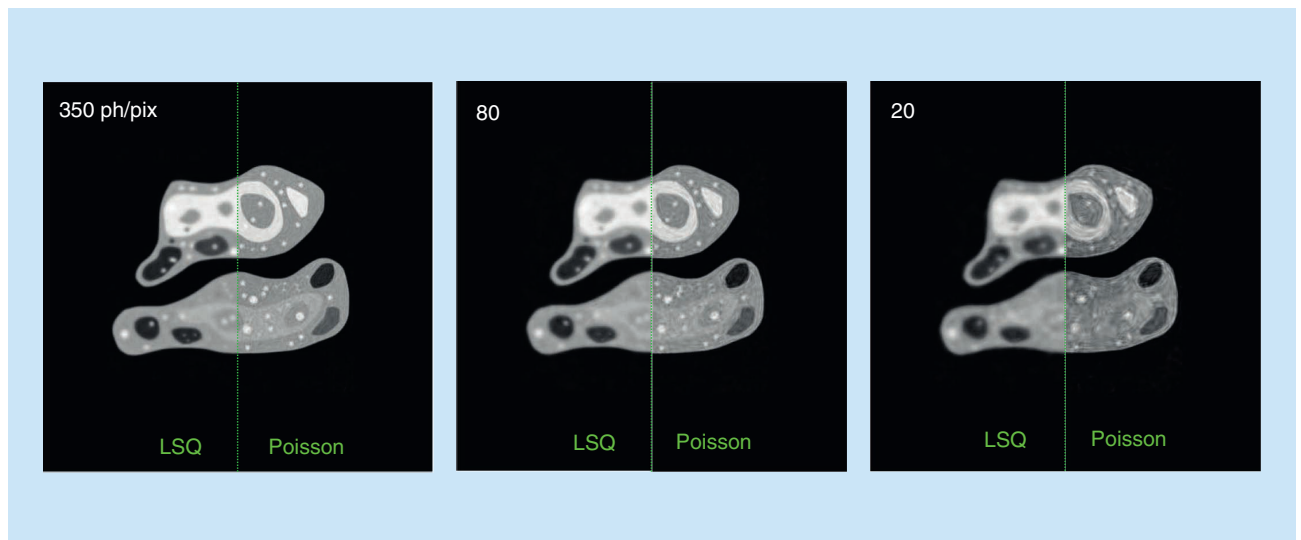


FIGURE 6. As the cumulative number of illuminating photons per pixel (ph/pix) (fluence) is reduced, the error metric used for image reconstruction should be changed from the least-squares (LSQ) model to that of (13) for Poisson statistics. This is illustrated here with a simulated cell object with a contrast such that one would expect a signal-to-noise ratio of 5:1 with a fluence of 350 ph/pix (or 9.2×10^7) photons distributed among 72×72 diffraction patterns). At that fluence, there is little difference between the LSQ and Poisson models, but at lower fluences of 80 and 20 ph/pix, one can see that the Poisson metric yields a sharper image [34].

problem in (13) into ptychography and tomography problems and solve alternatively, as previously explained, such as to parallelize the computations so as to shorten the time required for a solution.

Partial coherence of the illumination wave

The basic operation principle of ptychography relies heavily on the coherence of the illumination wave. However, in practice, high-frequency vibrations due to mechanical scanning or other experimental factors have the same effect as limiting the spatial coherence. Also, in some cases when faster imaging is desired, broadband illumination can be used to improve the fluence on the sample; this also leads to a degradation of the spectral coherence of the wave and eventually to worse results.

In these cases where we have a partially coherent source, the reconstructed images are blurred proportionally to the loss of coherence, unless compensated by applying established blind deconvolution methods. The process of deconvolution of motion from the image requires joint estimation of both the convolution kernels and the final image, and is often a data- and compute-intensive one. The corresponding problem can be defined by decomposing the probe function into multiple functions (also called *states* or *probe modes*) and requires solving a similar minimization problem as in (13). A common technique, known as *mixed-state* or *multiprobe decomposition*, employs this type of decomposition and models the measurement process using a linear combination of probe and object modes, which can be solved all together with existing reconstruction methods [37].

The process of deconvolution of motion from the image requires joint estimation of both the convolution kernels and the final image, and is often a data- and compute-intensive one.

Uncertainties in scan positions

Another important consideration is the presence of geometrical alignment errors requiring position correction in ptychography, and refinement of the image acquisition geometry in tomography. In ptychography, the location of the probe with respect to the sample is often not certain at the level of the targeted resolution; as a result, inaccurate scan locations induce artifacts and degrade quality in reconstructions [see Figure 7(a)]. A common approach is to treat probe locations t as unknowns and optimize those as a part of the image-reconstruction problem. An update of the locations is often performed in sample space, aiming to improve the consistency of locations or updated image patches. For example, when we consider the least-squares minimization problem

$\min_{Q,t,g} \|Q_t g - \psi\|_2^2$, we can alternatively solve for Q , t , and g in an approach similar to a block-coordinate descent method. Once the updates for Q and g are done, we can update t based on the cross correlation (or any other registration scheme) between object estimates at neighboring probe locations [28]. Optimization methods such as steepest descent have also been used for solving the registration problem and perform the position update for given Q and g [38]. In some cases, it is also adequate to regularize t (e.g., Tikhonov regularization) such that the recovered positions do not deviate too much from their expected locations.

Uncertainties in rotation angles

A similar geometrical alignment is required in tomography. Although the rotation angles of sample stages are usually quite precise, subsequent transverse positions of the rotation stage

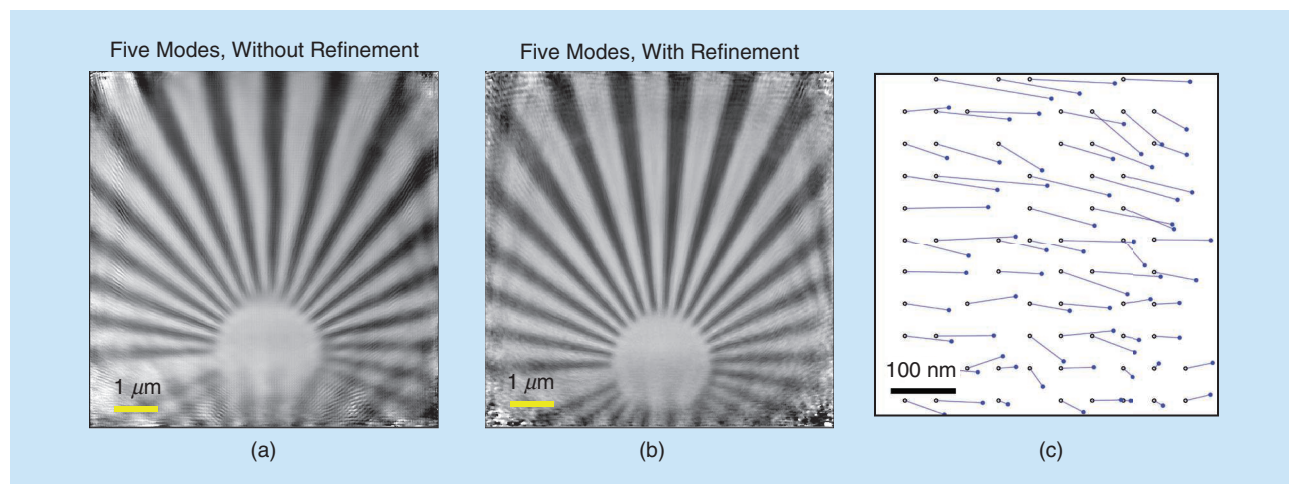


FIGURE 7. An example of the refinement of erroneous probe positions in ptychography. An X-ray ptychography data set was acquired with erroneous probe positions. (a) The ptychographic reconstruction obtained using the original, incorrect positions, (b) the image when the probe position refinement is applied, and (c) the change from incorrect (hollow black circles) to correct (solid blue circles) for a subset of the probe positions. This experiment also used a continuously moving probe, requiring the use of five probe modes to obtain a high-quality reconstruction [39]. The field of view of the ptychographic reconstruction extends beyond the original scanned illumination area, which is why image quality is low at the edges of the reconstructed images.

relative to the sample are not. In addition to random jitter in the rotation system, the stages may experience drift in time. Therefore, we need to align projections of the object for each angle such that all projections are consistent with each other around a common rotation axis. Mathematically speaking, we try to optimize the location of the image frames such that the following types of problems are solved:

$$\min_{f,p} \|R_\theta B_p f - g\|_2^2 \text{ or } \min_{f,p} \|B_p R_\theta f - g\|_2^2, \quad (14)$$

where B_p is a generic type of translation operator parameterized with p . The operators of this form can be applied either on the object [40] or the data [41] [the left- or right-hand problems in (14)]. However, when the sample is static, the right-hand problem is computationally favorable because each projection can be independently processed, and parallelization is more straightforward. Conversely, when the reconstructed object size is smaller than the data size (for example, in the case of undersampling), the size of the left-hand problem is potentially smaller. Similar to the position-correction problem in ptychography, iterative reprojection [42] or other types of optimization methods can be applied to solve this problem.

Depth-of-field problem

In the “Imaging of Thick Samples in 3D” section, it was assumed that the 2D projection g in (8) was sufficient to represent a 3D object when viewed from a particular angle. However, Fresnel propagation effects within the object means that one loses the validity of this simple projection approximation when the object’s thickness extends beyond a thickness equivalent to an optic’s depth of focus $\text{DOF} = (2/0.61^2) \delta_t^2 / \lambda \simeq 5.4 \delta_t^2 / \lambda$, where δ_t is the achieved transverse spatial resolution and λ is the wavelength of the beam [1]. The reconstruction approaches based on nonlinear optimization require only that one calculate from the present guess of the object the far-field intensities that one would measure (followed by minimization of the difference from the measured intensities) so that one can replace the simple projection model R_θ of (8) with a wave propagation model of how the illumination propagates through the guessed object and thus reconstruct objects that extend beyond the depth of focus, and that violate the first Born approximation. Although this approach has been demonstrated first in electron microscopy [43] and then in light and X-ray microscopy, the combination of the high penetrating power and short wavelength of X-rays means that this problem becomes especially acute as one scales up X-ray nanoimaging to larger objects such as, eventually, entire tissues (such as mouse brains in connectomics) [44].

Outlook and opportunities

A practical implementation of either ptychography or ptychotomography is challenging because of demanding computational requirements. For example, in a point-by-point scan, it is common to collect gigabytes of measurement data to recover a single megabyte image of the sample. Even for situations where

the image quality is compromised in favor of a quick scan, the data size is still selected to be roughly 10–20-times larger than the final image size. The data-acquisition rate of several tens of gigabytes⁻¹ is also high in ptychography with current photon-counting detectors. To be able to process data of this scale, implementations of popular algorithms like ePIE and DM on multicore architectures have been well established. These developments have made ptychography a more approachable technique for routine use at synchrotron facilities around the world. The common adoption of open source Python software libraries such as TensorFlow, PyTorch, and CuPy has made it easier to develop and validate new algorithms, helping to close the gap between algorithm design and high-performance computing implementations. In addition, although the classical approach of the “download first, then process” paradigm is still the mainstream practice of today, new real-time image processing frameworks that can reconstruct images as data are collected are being explored to achieve online steering of dynamical imaging experiments.

Although there are ptychography applications that consider adding prior information to constrain the solution set, applying regularization is often considered an exception rather than the rule in current applications. We believe there are potentially two reasons for this. First, most of the current ptychography experiments practice oversampling. Therefore, noise or other artifacts are not a main concern in the reconstruction process. However, this trend is changing with the emerging light sources. With the significantly improved spatial coherence of new sources, radiation dose is becoming the fundamental limit to achievable resolution; therefore, undersampling-based acquisition schemes and appropriate regularization strategies will possibly be an active field for future applications. Second, modifying existing implementations of mainstream algorithms is difficult because extensible frameworks are not widespread. There are current development efforts to provide hardware-agnostic interfaces for flexible yet high-performance implementations of reconstruction software on multiple compute resources.

Even though ptychography can provide very high spatial-resolution images, the time required to acquire those images is still high due to the inherent scanning procedure. Improving data-acquisition time through compressive-sensing methods will enable a range of capabilities that are very critical for materials science studies, including capturing dynamic phenomena under operando conditions or imaging larger sample volumes. All of the aforementioned procedures are now routinely done in electron microscopy and full-field X-ray microscopy but remain challenging for ptychography, which provides excellent opportunities for future development. For example, when capturing dynamic phenomena, the ability to study how materials respond to an external stimulus during processing or under operational conditions is critical to advance our understanding of nonequilibrium behaviors of materials. Moreover, imaging larger volumes is crucial not only for studying materials with proper statistics, it also offers opportunities to study heterogeneous and hierarchical structures where the nanoscale

features need to be studied on a tens-of-micrometers or even millimeters-length scale. Enhancing time resolution is therefore crucial to enable higher-dimensional analysis, such as carrying out ptychography as a function of incident X-ray energy for spectroscopic imaging [2].

To fully utilize high coherent flux sources, one can change from a “move–settle–acquire” sequence to continuous velocity scanning. For further time gains, there are alternative paths to follow: either we need to scan faster, or scan less. In the past, the target has been rapid scanning, and there have been high-precision mechanical engineering efforts for designing accurate scanning stages that can reliably operate at high scan speeds. The main challenge is that rapid scanning introduces high-frequency vibrations, which limits the spatial coherence of the source and blurs the collected images. The solution for this motion-deblurring problem requires developing methods that deconvolve the unknown spatiotemporally varying kernel from measurements. Because the number of unknown parameters that describe the motion is much higher than the object parameters, it is both an algorithmically and computationally challenging problem.

Another way to perform rapid imaging is to scan less and use compressive-sensing techniques to complement sparse acquisition. Although tomography enjoys developments in compressive sensing that enable it to greatly reduce the number of projections of the object, compressive sensing in ptychography is fundamentally difficult due to the necessary overlap constraint for solving the phase-retrieval problem. Also, in the case of continuous scanning, we cannot jump from one point to another point instantaneously; acceleration limits on optics and specimens demand continuous scanning. Therefore, it is difficult to design an acquisition scheme where we reduce the total length of the trajectory and acquire information uniformly across the whole image. In these conditions, sparse acquisition could be performed when we solve ptychography and tomography problems together. We can leverage compressive sensing for both problems, especially when we solve those problems jointly. However, we need to design a separate sparse-sampling trajectory for each rotation angle such that they complement each other when reconstructing the sample in 3D.

In the past, ML has demonstrated that deep neural networks can replace or complement regularized solutions to problems for a range of imaging tasks like denoising, inpainting, super-resolution, or deconvolution. In parallel, work on unsupervised methods showed how deep networks can outperform classical optimization techniques by constraining the reconstructed image to remain on a learned manifold. In addition to those studies, an ML-based approach can be used to constrain both/ either the likelihood and/or prior terms; these approaches can lead to a viable path to compressive sensing [45]. Although these types of joint-ML and physics-based solution approaches are getting more popular in tomography, ptychography applications are still in their infancy. This could be potentially related to the nonconvexity of the phase-retrieval problem in ptychography, which requires special attention in applying ML models. In addition, the training process grows proportion-

ally with the size of the degrees of freedom in the problem so that the application of ML methods to large-scale 3D imaging problems is still a challenge. Nevertheless, there are promising studies showing that ML-based regularization can allow for lifting the overlap constraint in ptychography. We believe that there are untapped potential uses of both trained and untrained deep networks for effectively constraining the solution set and enhancing the reconstructions.

Acknowledgments

We thank Hanfei Yan, Manuel Guizar-Sicarios, Maik Kahnt, Wendy Di, and two anonymous reviewers for their thoughtful comments and efforts toward improving this article. This research used resources of the Advanced Photon Source, a U.S. Department of Energy (DOE) Office of Science User Facility at Argonne National Laboratory, and is based on research supported by the U.S. DOE Office of Science-Basic Energy Sciences under contract DE-AC02-06CH11357. Yu-chen Karen Chen-Wiegart acknowledges support provided by the Faculty Early Career Development Program (CAREER) program and the Metals and Metallic Nanostructures program of the National Science Foundation under grant DMR-1752839.

Authors

Doğa Gürsoy (dgursoy@anl.gov) received his Ph.D. degree in electrical engineering from Graz University of Technology. He is with the Advanced Photon Source, Argonne National Laboratory, Lemont, Illinois, 60439, USA, and the Electrical Engineering and Computer Science Department, Northwestern University, Evanston, Illinois, 60208, USA. His research interests focus on computational imaging and inverse problems in imaging sciences.

Yu-chen Karen Chen-Wiegart (karen.chen-wiegart@stonybrook.edu) received her Ph.D. in materials science and engineering from Northwestern University. She is with the Materials Science and Chemical Engineering Department, Stony Brook University, Stony Brook, New York, 11794, USA, and National Synchrotron Light Source II, Brookhaven National Laboratory, Upton, New York, 11961, USA. Her research interests include energy storage and conversion, nano-/meso-porous materials, thin film and surface treatment, 3D printing/additive manufacturing and cultural heritage.

Chris Jacobsen (cjacobsen@anl.gov) received his Ph.D. in physics and astronomy from Stony Brook University. He is with the Advanced Photon Source, Argonne National Laboratory, Lemont, Illinois, 60439, USA, and the Physics and Astronomy Department, Northwestern University, Evanston, Illinois, 60208, USA. His research interests focus on developing new methods in X-ray microscopy and applying them to biological and materials science studies.

References

- [1] C. Jacobsen, *X-Ray Microscopy*. Cambridge, U.K.: Cambridge Univ. Press, 2020.
- [2] D. A. Shapiro, Y.-S. Yu, T. Tyliczszak, J. Cabana, R. Celestre, W. Chao, K. Kaznatcheev, A. L. D. Kilcoyne et al., “Chemical composition mapping with

- nanometre resolution by soft X-ray microscopy," *Nature Photonics*, vol. 8, no. 10, pp. 765–769, 2014, doi: 10.1038/nphoton.2014.207.
- [3] V. de Andrade, V. Nikitin, M. Wojcik, A. Deriy, S. Bean, D. Shu, T. Mooney, K. Peterson et al., "Fast X-ray nanotomography with sub-10 nm resolution as a powerful imaging tool for nanotechnology and energy storage applications," *Adv. Mater.*, vol. 33, no. 21, p. 2008653, 2021, doi: 10.1002/adma.202008653.
- [4] J. C. da Silva, A. Pacureanu, Y. Yang, S. Bohic, C. Morawe, R. Barrett, and P. Cloetens, "Efficient concentration of high-energy X-rays for diffraction-limited imaging resolution," *Optica*, vol. 4, no. 5, pp. 492–495, 2017, doi: 10.1364/OPTICA.4.000492.
- [5] D. Gürsoy and C. Jacobsen, "Multimodal X-ray nanotomography," *MRS Bull.*, vol. 45, no. 4, pp. 272–276, 2020, doi: 10.1557/mrs.2020.85.
- [6] M. Du and C. Jacobsen, "Relative merits and limiting factors for X-ray and electron microscopy of thick, hydrated organic materials," *Ultramicroscopy*, vol. 184, pp. 293–309, 2018, doi: 10.1016/j.ultramic.2017.10.003.
- [7] J. Deng, D. J. Vine, S. Chen, Q. Jin, Y. S. G. Nashed, T. Peterka, S. Vogt, and C. Jacobsen, "X-ray ptychographic and fluorescence microscopy of frozen-hydrated cells using continuous scanning," *Sci. Rep.*, vol. 7, no. 1, p. 445, 2017, doi: 10.1038/s41598-017-00569-y.
- [8] M. Holler, M. Odstrčil, M. Guizar-Sicairos, M. Lebugle, E. Müller, S. Finizio, G. Tinti, C. David et al., "Three-dimensional imaging of integrated circuits with macro- to nanoscale zoom," *Nature Electron.*, vol. 2, no. 10, pp. 464–470, Oct. 2019, doi: 10.1038/s41928-019-0309-z.
- [9] M. O. Hill, I. Calvo-Almazan, M. Allain, M. V. Holt, A. Ulvestad, J. Treu, G. Koblmüller, C. Huang et al., "Measuring three-dimensional strain and structural defects in a single InGaAs nanowire using coherent X-ray multiangle Bragg projection ptychography," *Nano Lett.*, vol. 18, no. 2, pp. 811–819, 2018, doi: 10.1021/acs.nanolett.7b04024.
- [10] M. Dierolf, A. Menzel, P. Thibault, P. Schneider, C. M. Kewish, R. Wepf, O. Bunk, and F. Pfeiffer, "Ptychographic X-ray computed tomography at the nanoscale," *Nature*, vol. 467, no. 7314, pp. 436–439, 2010, doi: 10.1038/nature09419.
- [11] S. Brisard, M. Serdar, and P. J. Monteiro, "Multiscale X-ray tomography of cementitious materials: A review," *Cement Concrete Res.*, vol. 128, p. 105824, 2020, doi: 10.1016/j.cemconres.2019.105824.
- [12] Z. Zhang, J. C. Khong, B. Koe, S. Luo, S. Huang, L. Qin, S. Cipiccia, D. Batey et al., "Multiscale characterization of the 3D network structure of metal carbides in a Ni superalloy by synchrotron X-ray microtomography and ptychography," *Scripta Materialia*, vol. 193, pp. 71–76, 2021, doi: 10.1016/j.scriptamat.2020.10.032.
- [13] Y.-C. Lin, X. Liu, K. W. Chou, E. H. Tsai, C. Zhao, M. Holler, A. Diaz, S. Petrasch et al., "Unveiling 3D morphology of multiscale micro-nanosilver sintering for advanced electronics manufacturing by ptychographic x-ray nanotomography," *Adv. Eng. Mater.*, vol. 22, no. 4, p. 1901250, 2020, doi: 10.1002/adem.201901250.
- [14] S. Müller, M. Lippuner, M. Vezzhak, V. De Andrade, F. De Carlo, and V. Wood, "Multimodal nanoscale tomographic imaging for battery electrodes," *Advanced Energy Materials*, vol. 10, no. 28, p. 1904119, 2020, doi: 10.1002/aenm.201904119.
- [15] V. Savikhin, D. A. Shapiro, X. Gu, S. D. Oosterhout, and M. F. Toney, "Ptychography of organic thin films at soft X-ray energies," *Chem. Mater.*, vol. 31, no. 13, pp. 4913–4918, 2019, doi: 10.1021/acs.chemmater.9b01690.
- [16] C. Donnelly, M. Guizar-Sicairos, V. Scagnoli, S. Gliga, M. Holler, J. Raabe, and L. J. Heyderman, "Three-dimensional magnetization structures revealed with X-ray vector nanotomography," *Nature*, vol. 547, no. 7663, pp. 328–331, 2017, doi: 10.1038/nature23006.
- [17] P. Godard, G. Carbone, M. Allain, F. Mastropietro, G. Chen, L. Capello, A. Diaz, T. H. Metzger et al., "Three-dimensional high-resolution quantitative microscopy of extended crystals," *Nature Commun.*, vol. 2, no. 1, p. 568, 2011, doi: 10.1038/ncomms1569.
- [18] J. Miao, P. Charalambous, J. Kirz, and D. Sayre, "Extending the methodology of X-ray crystallography to allow imaging of micrometre-sized non-crystalline specimens," *Nature*, vol. 400, no. 6742, pp. 342–344, 1999, doi: 10.1038/22498.
- [19] I. K. Robinson, I. A. Vartanyants, G. J. Williams, M. A. Pfeifer, and J. A. Pitney, "Reconstruction of the shapes of gold nanocrystals using coherent X-ray diffraction," *Phys. Rev. Lett.*, vol. 87, no. 19, p. 195505, Oct. 2001, doi: 10.1103/PhysRevLett.87.195505.
- [20] R. W. Gerchberg and W. O. Saxton, "A practical algorithm for the determination of phase from image and diffraction plane pictures," *Optik*, vol. 35, pp. 237–246, 1972.
- [21] J. R. Fienup, "Phase retrieval algorithms: A comparison," *Appl. Opt.*, vol. 21, no. 15, pp. 2758–2769, 1982, doi: 10.1364/AO.21.002758.
- [22] V. Elser, "Phase retrieval by iterated projections," *J. Opt. Soc. America A*, vol. 20, no. 1, pp. 40–55, 2003, doi: 10.1364/JOSA.A.20.000040.
- [23] B. L. M., "The method of successive projection for finding a common point of convex sets," *Soviet Mathematics Doklady*, vol. 162, no. 3, pp. 688–692, 1965.
- [24] J. Douglas and H. H. Rachford, "On the numerical solution of heat conduction problems in two and three space variables," *Trans. Amer. Math. Soc.*, vol. 82, no. 2, pp. 421–439, 1956, doi: 10.1090/S0002-9947-1956-0084194-4.
- [25] J. M. Rodenburg and H. M. L. Faulkner, "A phase retrieval algorithm for shifting illumination," *Appl. Phys. Lett.*, vol. 85, no. 20, pp. 4795–4797, 2004, doi: 10.1063/1.1823034.
- [26] P. Thibault, M. Dierolf, A. Menzel, O. Bunk, C. David, and F. Pfeiffer, "High-resolution scanning X-ray diffraction microscopy," *Science*, vol. 321, no. 5887, pp. 379–382, 2008, doi: 10.1126/science.1158573.
- [27] A. M. Maiden and J. M. Rodenburg, "An improved ptychographical phase retrieval algorithm for diffractive imaging," *Ultramicroscopy*, vol. 109, no. 10, pp. 1256–1262, 2009, doi: 10.1016/j.ultramic.2009.05.012.
- [28] M. Guizar-Sicairos and J. R. Fienup, "Phase retrieval with transverse translation diversity: A nonlinear optimization approach," *Optics Express*, vol. 16, no. 10, pp. 7264–7278, 2008, doi: 10.1364/OE.16.007264.
- [29] D. Gürsoy, "Direct coupling of tomography and ptychography," *Optics Lett.*, vol. 42, no. 16, pp. 3169–3172, 2017, doi: 10.1364/OL.42.003169.
- [30] M. Kahnt, J. Becher, D. Brückner, Y. Fam, T. Sheppard, T. Weissenberger, F. Wittwer, J.-D. Grunwaldt et al., "Coupled ptychography and tomography algorithm improves reconstruction of experimental data," *Optica*, vol. 6, no. 10, pp. 1282–1289, 2019, doi: 10.1364/OPTICA.6.001282.
- [31] R. Hegerl and W. Hoppe, "Influence of electron noise on three-dimensional image reconstruction," *Zeitschrift für Naturforschung A*, vol. 31, no. 12, pp. 1717–1721, 1976, doi: 10.1515/zna-1976-1241.
- [32] S. Aslan, V. Nikitin, D. J. Ching, T. Bicer, S. Leyffer, and D. Gürsoy, "Joint ptycho-tomography reconstruction through alternating direction method of multipliers," *Optics Express*, vol. 27, no. 6, pp. 9128–9143, 2019, doi: 10.1364/OE.27.009128.
- [33] H. Yan, "Ptychographic phase retrieval by proximal algorithms," *New J. Phys.*, vol. 22, no. 2, p. 023035, 2020, doi: 10.1088/1367-2630/ab704e.
- [34] M. Du, D. Gürsoy, and C. Jacobsen, "Near, far, wherever you are: Simulations on the dose efficiency of holographic and ptychographic coherent imaging," *J. Appl. Crystallogr.*, vol. 53, no. 3, 2020, doi: 10.1107/S1600576720005816.
- [35] P. Thibault and M. Guizar-Sicairos, "Maximum-likelihood refinement for coherent diffractive imaging," *New J. Phys.*, vol. 14, no. 6, p. 063004, 2012, doi: 10.1088/1367-2630/14/6/063004.
- [36] V. Nikitin, S. Aslan, Y. Yao, T. Biçer, S. Leyffer, R. Mokso, and D. Gürsoy, "Photon-limited ptychography of 3D objects via Bayesian reconstruction," *OSA Continuum*, vol. 2, no. 10, pp. 2948–2968, 2019, doi: 10.1364/OSAC.2.002948.
- [37] P. Thibault and A. Menzel, "Reconstructing state mixtures from diffraction measurements," *Nature*, vol. 494, no. 7435, p. 68, 2013, doi: 10.1038/nature11806.
- [38] P. Dwivedi, A. Konijnenberg, S. Pereira, and H. Urbach, "Lateral position correction in ptychography using the gradient of intensity patterns," *Ultramicroscopy*, vol. 192, pp. 29–36, 2018, doi: 10.1016/j.ultramic.2018.04.004.
- [39] M. Du, S. Kandel, J. Deng, X. Huang, A. Demortière, T. T. Nguyen, R. Tucoulou, V. De Andrade et al., "Adorym: A multi-platform generic X-ray image reconstruction framework based on automatic differentiation," *Optics Express*, vol. 29, no. 7, pp. 10,000–10,035, Mar. 2021, doi: 10.1364/OE.418296.
- [40] M. Odstrčil, M. Holler, J. Raabe, A. Sepe, X. Sheng, S. Vignolini, C. G. Schroer, and M. Guizar-Sicairos, "Ab initio nonrigid X-ray nanotomography," *Nature Commun.*, vol. 10, no. 1, p. 2600, 2019, doi: 10.1038/s41467-019-10670-7.
- [41] V. Nikitin, V. De Andrade, A. Slyamov, B. J. Gould, Y. Zhang, V. Sampathkumar, N. Kasthuri, D. Gürsoy et al., "Distributed optimization for nonrigid nano-tomography," *IEEE Trans. Comput. Imaging*, vol. 7, pp. 272–287, 2021, doi: 10.1109/TCLI.2021.3060915.
- [42] D. Gürsoy, Y. P. Hong, K. He, K. Hujsak, S. Yoo, S. Chen, Y. Li, M. Ge et al., "Rapid alignment of nanotomography data using joint iterative reconstruction and reprojection," *Sci. Rep.*, vol. 7, no. 1, p. 11,818, 2017, doi: 10.1038/s41598-017-12141-9.
- [43] W. V. d Broek and C. T. Koch, "Method for retrieval of the three-dimensional object potential by inversion of dynamical electron scattering," *Phys. Rev. Lett.*, vol. 109, no. 24, p. 245,502, 2012, doi: 10.1103/PhysRevLett.109.245502.
- [44] M. Du, Z. Di, D. Gürsoy, P. Xian, Y. Kozorovitskiy, and C. Jacobsen, "Upscaling X-ray nanoimaging to macroscopic specimens," *J. Appl. Crystallogr.*, vol. 54, no. 2, 2021, doi: 10.1107/S1600576721000194.
- [45] S. Aslan, Z. Liu, V. Nikitin, T. Bicer, S. Leyffer, and D. Gürsoy, "Joint ptycho-tomography with deep generative priors," *Mach. Learning: Sci. Technol.*, vol. 2, no. 4, 2021, doi: 10.1088/2632-2153/ac1d35.

